

Probing the QCD Critical End Point with Finite-Size Scaling of Net-Baryon Cumulant Ratios

Roy A. Lacey^{1,*}

¹*Department of Chemistry, Stony Brook University,
Stony Brook, NY, 11794-3400, USA*

(Dated: November 26, 2024)

The search for the Quantum Chromodynamics (QCD) critical end point (CEP) is a central focus in heavy-ion physics, as it provides insights into the phase structure of strongly interacting matter under extreme conditions. Finite-size scaling (FSS) analysis is applied to explore the critical behavior of cumulant ratios C_2/C_1 , C_3/C_2 , C_4/C_2 , C_3/C_1 , and C_4/C_1 , measured in Au+Au collisions across the Beam Energy Scan (BES) range of 7.7 to 200 GeV. The inferred CEP from the FSS analysis is located at $\sqrt{s}_{\text{CEP}} \approx 33.0$ GeV, corresponding to $\mu_{B,\text{CEP}} \approx 130$ MeV and $T_{\text{CEP}} \approx 158.5$ MeV, as derived from the freeze-out curve. The scaling functions for these cumulant ratios reveal non-monotonic patterns, where critical fluctuations manifest as distinct scaling behaviors. Specifically, the FSS analysis demonstrates upward divergence of C_2/C_1 and C_4/C_1 , and downward divergence of C_3/C_2 and C_4/C_2 , consistent with theoretical expectations for critical dynamics near the CEP. These findings validate the robustness of these cumulant ratios as effective probes for critical phenomena, offering structured evidence for the inferred CEP in QCD matter.

PACS numbers: 25.75.-q, 25.75.Dw, 25.75.Ld

The search for the Quantum Chromodynamics (QCD) critical end point (CEP) is a key objective in heavy-ion physics, offering insights into the behavior of strongly interacting matter under extreme conditions. The CEP marks the boundary between a first-order phase transition and a smooth crossover in the QCD phase diagram, analogous to the liquid-gas critical point in water [1, 2].

To probe the CEP, heavy-ion collision experiments, such as the Beam Energy Scan (BES) program at the Relativistic Heavy Ion Collider (RHIC), measure variations in cumulants of the net-baryon number distribution across a range of collision energies and for several centralities at each beam energy [3]. Cumulants are statistical measures that describe the shape of a distribution, capturing moments such as the mean (first-order cumulant, C_1), variance (second-order cumulant, C_2), skewness (third-order cumulant, C_3), and kurtosis (fourth-order cumulant, C_4). While lower-order cumulants, like C_1 and C_2 , reflect basic properties such as the mean and variance, higher-order cumulants, such as C_3 and C_4 , are particularly sensitive to non-Gaussian behavior. Ratios of these cumulants, such as C_2/C_1 , C_3/C_2 , and C_4/C_2 , are expected to exhibit monotonic energy dependence under non-critical conditions. However, deviations from these monotonic trends, particularly non-monotonic behavior, provide valuable insights into critical fluctuations associated with the CEP.

Identifying the CEP in heavy-ion collisions presents notable challenges due to finite-size and finite-time effects that can dampen or distort signatures of criticality. In finite systems, true phase transitions are replaced by smooth crossovers, limiting the development of long-wavelength modes that are crucial for observable critical fluctuations. Additionally, the short-lived nature of the fireball means there is insufficient time for long-wavelength fluctuations to fully develop, which restricts the correlation length and limits the extent of critical fluctuations, complicating experimental detection.

Direct observation of non-monotonic patterns in cumulant ratios, as might be expected in the beam energy dependence of raw data, is challenging due to the combined constraints of finite size and finite time. Finite-size scaling (FSS) offers a framework to interpret the scaling behavior of these ratios effectively when finite-time effects are not dominant. FSS can help uncover non-monotonic signals when finite-size effects are significant, though finite-time constraints may moderate these characteristics. Conversely, when finite-time effects dominate, the growth of correlation lengths and the emergence of critical signals may be significantly suppressed [4], impacting their visibility even with FSS. Ratios such as C_2/C_1 and C_3/C_2 , which benefit from volume cancellation, are relatively resilient to finite-time effects because they capture lower-order fluctuations that develop more rapidly than higher-order, non-Gaussian fluctuations. This resilience supports their utility in extracting susceptibility curves and enhancing the search for the CEP by providing robust insights into critical responses [5].

Non-perturbative QCD structures, such as baryon junctions, could play a crucial role in enhancing cumulant ratios like C_2/C_1 , C_3/C_2 , and higher-order ratios such as C_4/C_2 through increased baryon stopping at lower beam energies [6–9]. These structures promote substantial baryon density fluctuations by facilitating the transfer of baryon number to mid-rapidity, particularly in regions of the QCD phase diagram where baryon stopping is pronounced [9]. Near the CEP, such fluctuations could seed critical dynamics, amplifying compressibility, skewness, and kurtosis as captured by these cumulant ratios [5, 10]. While baryon junctions offer potential advantages as amplifiers of critical signals, they may also generate non-critical density fluctuations that could complicate the interpretation of CEP-related effects, underscoring the importance of future theoretical efforts to disentangle these effects and their role in CEP studies.

Finite-size scaling is essential for understanding the scaling

behavior of cumulant ratios in heavy-ion collisions, helping to identify genuine critical phenomena and distinguish them from finite-size artifacts. Near the CEP, cumulant ratios follow the FSS relations [11]:

$$\begin{aligned} \frac{C_2}{C_1} &= L^{\gamma/\nu} f_{21}(tL^{1/\nu}, hL^{\Delta/\nu}), & \frac{C_3}{C_2} &= L^{-\gamma/\nu} f_{32}(tL^{1/\nu}, hL^{\Delta/\nu}), \\ \frac{C_4}{C_2} &= L^{-\gamma/\nu} f_{42}(tL^{1/\nu}, hL^{\Delta/\nu}), & \frac{C_3}{C_1} &= L^{-(d-\gamma)/\nu} f_{31}(tL^{1/\nu}, hL^{\Delta/\nu}), \\ \frac{C_4}{C_1} &= L^{(d+\alpha)/\nu} f_{41}(tL^{1/\nu}, hL^{\Delta/\nu}), \end{aligned}$$

where L represents the system size, generally proportional to the fireball volume in heavy-ion collisions, and $t = (T - T_{\text{CEP}})/T_{\text{CEP}}$ is the reduced temperature with T_{CEP} as the critical temperature. The external field $h = (\mu_B - \mu_{B,\text{CEP}})/\mu_{B,\text{CEP}}$ is defined via the baryon chemical potential μ_B and its critical value $\mu_{B,\text{CEP}}$. Here, d is the spatial dimensionality, and γ , ν , α , and Δ are critical exponents that define the scaling behavior. The functions f_{21} , f_{32} , f_{42} , f_{31} , and f_{41} are universal scaling functions associated with each cumulant ratio.

This FSS framework provides a structured approach to studying critical behavior in finite systems, such as the hot, dense fireball produced in heavy-ion collisions near the QCD critical end point. Applying FSS across multiple cumulant ratios strengthens the reliability of CEP identification by enhancing insights into the critical fluctuations in QCD matter. By comparing density-driven and field-driven scaling paths, FSS confirms the universality of the CEP, as both approaches are expected to converge on the same location for the CEP. Furthermore, FSS enables assessment of the impact of finite-time effects on scaling fidelity, allowing for a more accurate interpretation of scaling signals and reinforcing the robustness of CEP identification.

Distinct cumulant ratios— C_2/C_1 , C_3/C_2 , C_3/C_1 , C_4/C_1 , and C_4/C_2 —provide essential insights into the critical dynamics near the CEP. Ratios such as C_2/C_1 and C_3/C_2 , which benefit from volume cancellation, are particularly robust for FSS analyses and serve as intensive quantities effective in detecting criticality signals. The upward divergence of C_2/C_1 , related to increasing susceptibility, reflects system compressibility as it approaches the CEP. Conversely, C_3/C_2 , associated with skewness, diverges downward, capturing asymmetry in the fluctuation distribution and highlighting non-Gaussian features.

The ratio C_4/C_2 , also benefiting from volume cancellation, is sensitive to higher-order non-Gaussian fluctuations and is expected to diverge downward near the CEP, though it may be more susceptible to finite-time effects due to the time required for such fluctuations to develop fully.

Higher-order ratios, C_3/C_1 and C_4/C_1 , provide further perspectives on critical behavior. Although only partially volume-cancelled, C_4/C_1 displays an upward divergence related to kurtosis and non-Gaussian fluctuations, while C_3/C_1

diverges downward, reflecting suppression of skewness relative to the mean. The partial volume cancellation in these ratios may affect their sensitivity to critical dynamics, yet they still contribute valuable information.

By analyzing these cumulant ratios together, scaling studies gain reliability and enhance CEP identification by ensuring each ratio's unique scaling behavior is used to build a comprehensive picture of the critical response near the CEP.

The size parameter $\bar{R} = L$ used in FSS analysis is derived from Monte Carlo Glauber (MC-Glauber) calculations [12, 13] for various collision centralities at each beam energy, detailing the nuclear geometry involved in each collision. In the MC-Glauber model, nucleons participating in an initial inelastic nucleon-nucleon (N+N) interaction form the participant set (N_{part}).

The transverse distribution of these participants in the X-Y plane is quantified by the root-mean-square (RMS) widths σ_x and σ_y , calculated along the principal axes of the participant zone. The transverse system size, \bar{R} , is then defined as $\frac{1}{\bar{R}} = \sqrt{\left(\frac{1}{\sigma_x^2} + \frac{1}{\sigma_y^2}\right)}$ [14], ensuring a meaningful representation of the system's geometric spread.

For FSS, the **relative magnitudes** of L across different energies and centralities are crucial, allowing for robust scaling analyses that account for possible model uncertainties in the absolute size of L . This approach facilitates the comparison of systems of varying sizes while maintaining the integrity of universal scaling behavior.

The parameter \bar{R} encapsulates the spatial extent of the colliding system. The three HBT radii— R_{out} , R_{side} , and R_{long} —characterize the space-time dimensions of the emitting sources and show a linear dependence on \bar{R} across the studied beam energy range [15, 16]. This consistency supports \bar{R} as a reliable measure of transverse size in FSS studies.

Systematic uncertainties for \bar{R} from varying model parameters within the MC-Glauber framework are estimated at less than 2% [13], confirming the robustness of \bar{R} for scaling analyses across centralities and beam energies. Consequently, \bar{R} serves as a practical metric for probing universal scaling in heavy-ion collisions.

To apply finite-size scaling relations to experimental data, the cumulant ratios C_2/C_1 , C_3/C_2 , C_4/C_2 , C_3/C_1 , and C_4/C_1 , measured in Au+Au collisions across the full Beam Energy Scan (BES) range from 7.7 to 200 GeV, are utilized [19]. The data spans several collision centralities, providing a comprehensive view of scaling behavior across varying system sizes. These ratios, sensitive to critical fluctuations, serve as effective probes for examining the QCD critical end point through their FSS properties.

Effective application of the FSS relations requires a clear understanding of the thermodynamic scaling variables—the reduced temperature t and external field h —that define the trajectory toward the CEP. However, directly accessing t and h is challenging in heavy-ion collisions. Beam energy (\sqrt{s}), serving as a practical proxy for both μ_B and T , allows these variables to be expressed in terms of \sqrt{s} , enabling system-

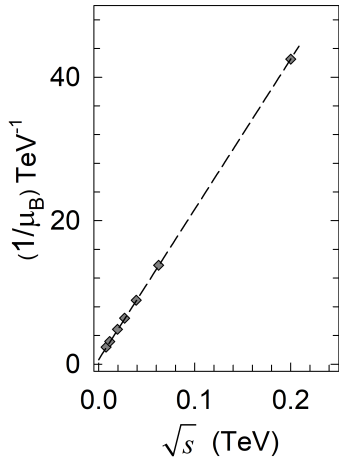


FIG. 1. (Color Online) The relationship between $1/\mu_B$ and beam energy (\sqrt{s}). The μ_B values are extracted from the freeze-out curve as parametrized in [17, 18], illustrating the approximate proportionality $1/\mu_B \propto \sqrt{s}$.

atic exploration of thermodynamic conditions. By leveraging the freeze-out curve to parametrize a path close to the CEP, \sqrt{s} reflects both density-driven and field-driven trajectories. Field-driven dynamics are especially relevant for observables sensitive to μ_B , such as net-baryon fluctuations, where critical scaling behavior emerges.

- *Field-Driven Scaling Variable $h_{\sqrt{s}}$* : Net-baryon fluctuations, dominated by field-driven dynamics and sensitive to variations in μ_B [20, 21], are analyzed using the field-driven scaling variable $h_{\sqrt{s}}$:

$$h_{\sqrt{s}} = \frac{(1/\mu_B) - (1/\mu_{B,CEP})}{(1/\mu_{B,CEP})}.$$

Here, $1/\mu_B \propto \sqrt{s}$, as illustrated in Fig. 1, which shows the linear relationship between \sqrt{s} and $1/\mu_B$ derived from the freeze-out curve [17, 18].

FSS with $h_{\sqrt{s}}$ extracts the critical beam energy \sqrt{s}_{CEP} by achieving scaling collapse across cumulant ratios (e.g., C_2/C_1 , C_3/C_2). This \sqrt{s}_{CEP} is then mapped to $\mu_{B,CEP}$ and T_{CEP} using the same freeze-out parametrization [17, 18].

The scaling collapse achieved with $h_{\sqrt{s}}$ demonstrates robust fidelity for extracting the critical beam energy \sqrt{s}_{CEP} . However, incorporating the inferred $\mu_{B,CEP}$ back into the field-driven scaling expression can lead to reduced scaling fidelity. This seeming discrepancy arises because \sqrt{s} , serving as a direct experimental proxy, inherently captures the relationship between beam energy and net-baryon fluctuations more effectively than the inferred thermodynamic variable $\mu_{B,CEP}$. Consequently, \sqrt{s} provides a more reliable basis for field-driven scaling, underscoring the need for careful validation of $\mu_{B,CEP}$ in scaling analyses.

- *Density-Driven Scaling Variable $t_{\sqrt{s}}$* : For density-driven scaling, the variable $t_{\sqrt{s}}$ is defined as:

$$t_{\sqrt{s}} = \frac{\sqrt{s} - \mu_{B,CEP}}{\mu_{B,CEP}}.$$

This definition explicitly incorporates $\mu_{B,CEP}$, leveraging the dominance of μ_B over the energy range of interest and the proportionality $1/\mu_B \propto \sqrt{s}$. Here, \sqrt{s} serves as a practical proxy for μ_B , but the scaling analysis explicitly validates $\mu_{B,CEP}$ derived from field-driven scaling.

To confirm scaling fidelity with $t_{\sqrt{s}}$, the critical $\mu_{B,CEP}$ inferred from $h_{\sqrt{s}}$ is used, ensuring consistency between density- and field-driven dynamics. This approach allows $t_{\sqrt{s}}$ to focus on deviations from $\mu_{B,CEP}$, linking density-driven scaling directly to the field-driven outcomes.

This dual approach—starting with $h_{\sqrt{s}}$ to determine \sqrt{s}_{CEP} and mapping it to $\mu_{B,CEP}$, followed by validation with $t_{\sqrt{s}}$ —provides a robust framework for estimating the CEP. By integrating field- and density-driven dynamics, this analysis leverages \sqrt{s} as a unified experimental proxy, yielding a reliable determination of the CEP in both temperature and chemical potential space.

Figures 2 and 3 illustrate the scaling procedure for C_2/C_1 and C_3/C_2 , respectively. Figs. 2 (a) and 3 (a) show that finite-time and finite-size effects mask the non-monotonic patterns that would indicate the CEP. By contrast, Figs. 2(b) and (c) and Figs. 3(b) and (c) reveal clear indications of non-monotonic patterns in the scaling functions, reflecting the upward divergence of C_2/C_1 (linked to increasing compressibility and susceptibility) and the downward divergence of C_3/C_2 (indicating skewness and asymmetry in fluctuations). The scaling fidelity for C_2/C_1 is high for both density- and field-driven scaling, suggesting limited influence from finite-time effects for this ratio. The fidelity for C_3/C_2 is also good but somewhat lower than for C_2/C_1 , possibly indicating the expected greater influence of finite-time effects on C_3/C_2 . Notably, the scaling behavior for proxy compressibility data reported in [5] shows similarly robust scaling functions, yielding values of $\mu_{B,CEP}$ and T_{CEP} consistent with those derived in the present analysis.

Figure 4 shows the field-driven scaling functions for C_4/C_2 , C_3/C_1 , and C_4/C_1 . Panel (a) shows the expected downward divergence near the CEP for C_4/C_2 , tied to higher-order, non-Gaussian fluctuations. This divergence may be of smaller magnitude, possibly due to finite-time effects. Panel (b) also shows the anticipated downward divergence near the CEP for C_3/C_1 , reflecting skewness suppression, but with reduced scaling fidelity, likely due to partial volume cancellation. In contrast, panel (c) shows the expected upward divergence near the CEP for C_4/C_1 , highlighting the contribution of kurtosis and non-Gaussian fluctuations, with relatively good scaling fidelity.

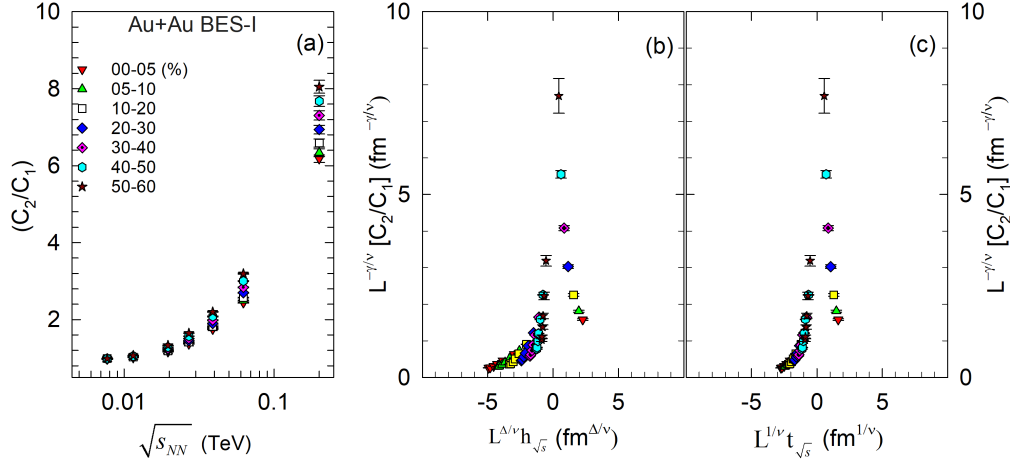


FIG. 2. (Color Online) Panel (a) presents the beam energy dependence of $C_2(\text{cent})/C_1(\text{cent})$ for Au+Au collisions across multiple centralities, as indicated. Panels (b) and (c) display the resulting field-driven and density-driven scaling functions obtained through finite-size scaling of the data in panel (a). The scaling functions exhibit the anticipated upward divergence in the vicinity of the CEP.

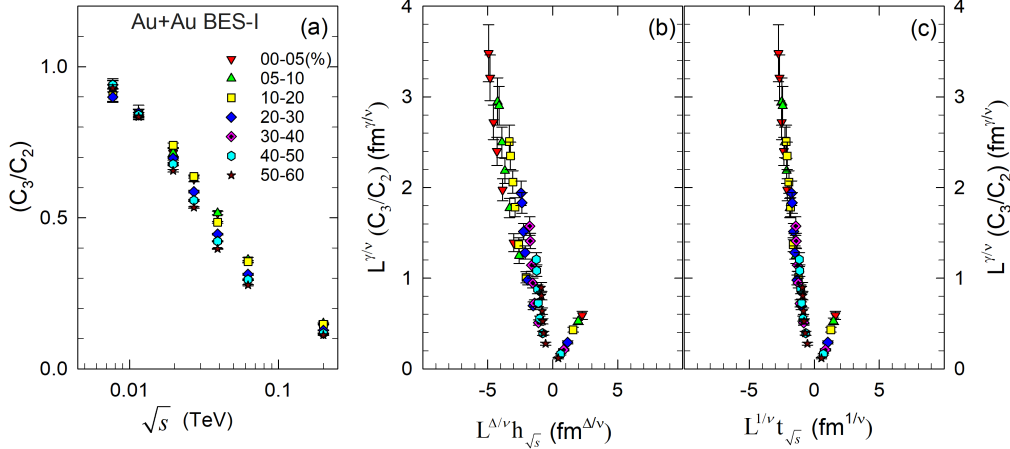


FIG. 3. (Color Online) Panel (a) presents the beam energy dependence of $C_3(\text{cent})/C_2(\text{cent})$ for Au+Au collisions across multiple centralities, as indicated. Panels (b) and (c) display the resulting field-driven and density-driven scaling functions obtained through finite-size scaling of the data in panel (a). The scaling functions exhibit the anticipated downward asymmetric divergence in the vicinity of the CEP.

The scaling functions presented in Figs. 1 - 4 were all obtained using $\sqrt{s}_{\text{CEP}} \approx 33.0$ GeV. The corresponding values, $\mu_{B,\text{CEP}} \approx 130$ MeV and $T_{\text{CEP}} \approx 158.5$ MeV, derived from the freeze-out curve [17, 18], establish a consistent thermodynamic reference for critical fluctuations. The finite-size scaling (FSS) framework, which systematically incorporates system size through scaling variables and functions, ensures that finite-time and finite-volume effects are accounted for. This approach leverages the distinct scaling behavior of each cumulant ratio to enhance the reliability of the analysis and provide robust support for CEP identification.

In summary, the finite-size scaling analysis of cumulant ratios C_2/C_1 , C_3/C_2 , C_4/C_2 , C_3/C_1 , and C_4/C_1 measured in Au+Au collisions across the BES energy range provides a compelling framework for locating the QCD critical end

point. The scaling behavior observed for these ratios, particularly the upward divergence of C_2/C_1 and C_4/C_1 and the downward divergence of C_3/C_2 and C_4/C_2 , aligns with theoretical expectations for critical dynamics near the CEP. The analysis, anchored at $\sqrt{s}_{\text{CEP}} = 33.0$ GeV and corresponding to $\mu_{B,\text{CEP}} \approx 130$ MeV and $T_{\text{CEP}} \approx 158.5$ MeV, offers a consistent reference across both field-driven and density-driven scaling variables. Moreover, the scaling fidelity observed, despite finite-time effects, underscores the robustness of these cumulant ratios as probes of critical behavior. Together, these findings enhance the reliability of CEP identification and contribute valuable insights into the critical fluctuations in strongly interacting matter, supporting further exploration in the quest to understand the QCD phase structure.

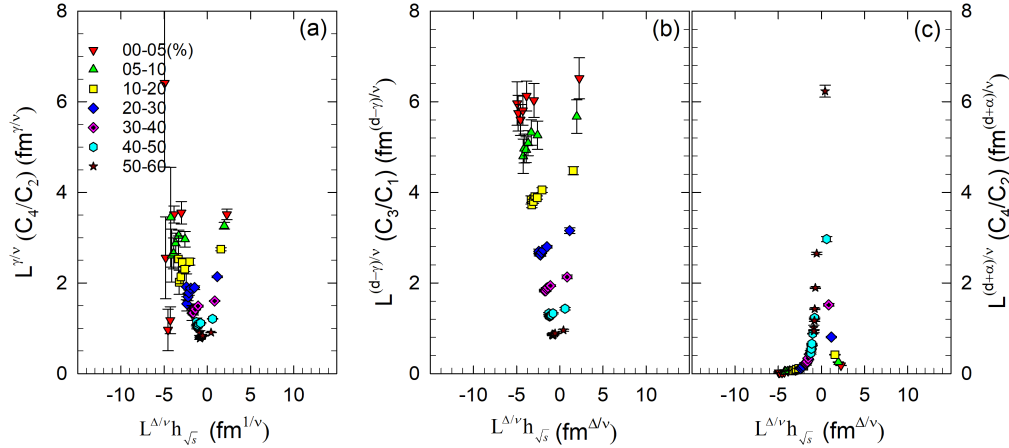


FIG. 4. (Color Online) Panels (a), (b), and (c) display the field-driven scaling functions obtained through finite-size scaling of the data for $C_4(\text{cent})/C_2(\text{cent})$, $C_3(\text{cent})/C_1(\text{cent})$, and $C_4(\text{cent})/C_1(\text{cent})$, respectively. The scaling functions exhibit the anticipated divergences in the vicinity of the CEP.

* E-mail: Roy.Lacey@Stonybrook.edu

- [1] M. A. Stephanov, *Prog. Theor. Phys. Suppl.* **153**, 139 (2004), [arXiv:hep-ph/0402115](#).
- [2] K. Rajagopal and F. Wilczek, “The Condensed matter physics of QCD,” in *At the frontier of particle physics. Handbook of QCD. Vol. 1-3*, edited by M. Shifman and B. Ioffe (2000) pp. 2061–2151, [arXiv:hep-ph/0011333](#).
- [3] J. Adam *et al.* (STAR), *Phys. Rev. Lett.* **126**, 092301 (2021), [arXiv:2001.02852 \[nucl-ex\]](#).
- [4] S. Mukherjee, R. Venugopalan, and Y. Yin, *Nucl. Phys. A* **967**, 820 (2017), [arXiv:1704.05427 \[hep-ph\]](#).
- [5] R. A. Lacey, *Phys. Rev. Lett.* **114**, 142301 (2015), [arXiv:1411.7931 \[nucl-ex\]](#).
- [6] D. Kharzeev, *Phys. Lett. B* **378**, 238 (1996), [arXiv:nucl-th/9602027](#).
- [7] D. Kharzeev and M. Nardi, *Phys. Lett. B* **507**, 121 (2001), [arXiv:nucl-th/0012025](#).
- [8] G. Pihan, A. Monnai, B. Schenke, and C. Shen, (2024), [arXiv:2405.19439 \[nucl-th\]](#).
- [9] R. A. Lacey, (2024), [arXiv:2410.22688 \[nucl-ex\]](#).
- [10] M. A. Stephanov, *Phys. Rev. Lett.* **102**, 032301 (2009), [arXiv:0809.3450 \[hep-ph\]](#).
- [11] J. Cardy, *Scaling and Renormalization in Statistical Physics*, Cambridge Lecture Notes in Physics (Cambridge University Press, Cambridge, UK, 1996).
- [12] M. L. Miller, K. Reygers, S. J. Sanders, and P. Steinberg, *Ann. Rev. Nucl. Part. Sci.* **57**, 205 (2007), [arXiv:nucl-ex/0701025](#).
- [13] R. A. Lacey, R. Wei, N. N. Ajitanand, and A. Taranenko, *Phys. Rev. C* **83**, 044902 (2011), [arXiv:1009.5230 \[nucl-ex\]](#).
- [14] R. S. Bhalerao, J.-P. Blaizot, N. Borghini, and J.-Y. Ollitrault, *Phys. Lett. B* **627**, 49 (2005), [arXiv:nucl-th/0508009](#).
- [15] R. A. Lacey, *Nucl. Phys. A* **931**, 904 (2014), [arXiv:1408.1343 \[nucl-ex\]](#).
- [16] A. Adare *et al.* (PHENIX), (2014), [arXiv:1410.2559 \[nucl-ex\]](#).
- [17] J. Cleymans, H. Oeschler, K. Redlich, and S. Wheaton, *Phys. Rev. C* **73**, 034905 (2006), [arXiv:hep-ph/0511094](#).
- [18] A. Andronic *et al.*, *Nucl. Phys. A* **837**, 65 (2010), [arXiv:0911.4806 \[hep-ph\]](#).
- [19] M. Abdallah *et al.* (STAR), *Phys. Rev. C* **104**, 024902 (2021), [arXiv:2101.12413 \[nucl-ex\]](#).
- [20] M. Asakawa, U. W. Heinz, and B. Muller, *Phys. Rev. Lett.* **85**, 2072 (2000), [arXiv:hep-ph/0003169](#).
- [21] M. A. Stephanov, *J. Phys. G* **38**, 124147 (2011).